




Measurement of four-photon absorption in GaP and ZnTe semiconductors

B. MONOSZLAI,^{1,2,6} P. S. NUGRAHA,^{1,3} GY. TÓTH,⁴ GY. POLÓNYI,^{1,3} L. PÁLFALVI,⁴ L. NASI,¹ Z. OLLMANN,⁵ E. J. ROHWER,⁵ G. GÄUMANN,⁵ J. HEBLING,^{1,3,4} T. FEURER,⁵ AND J. A. FÜLÖP^{1,2,3,*} 

¹Szentágotthai Research Centre, University of Pécs, 7624 Pécs, Hungary

²ELI-ALPS, ELI-Hu Nonprofit Ltd., 6720 Szeged, Hungary

³MTA-PTE High-Field Terahertz Research Group, 7624 Pécs, Hungary

⁴Institute of Physics, University of Pécs, 7624 Pécs, Hungary

⁵Institute of Applied Physics, University of Bern, 3012 Bern, Switzerland

⁶Current affiliation: European XFEL, 22869 Schenefeld, Germany

*fulop@fizika.ttk.pte.hu

Abstract: Intensity-dependent effective four-photon absorption (4PA) coefficients in GaP and ZnTe semiconductors were measured by the z-scan method using pump pulses of 1.75 μm wavelength, 135 fs duration, and up to 500 GWcm^{-2} intensity. A nonlinear pulse propagation model, including linear dispersion and 4PA was used to obtain the 4PA coefficients from measurements. The intensity-dependent effective 4PA coefficients vary from 2.6×10^{-4} to $65 \times 10^{-4} \text{ cm}^5 \text{GW}^{-3}$ in GaP, and from 3.5×10^{-4} to $9.1 \times 10^{-4} \text{ cm}^5 \text{GW}^{-3}$ in ZnTe. The anisotropy in 4PA was shown in GaP. The knowledge of 4PA coefficients is important for the design of semiconductor photonics devices.

© 2020 Optical Society of America under the terms of the [OSA Open Access Publishing Agreement](#)

1. Introduction

Semiconductor materials have been playing an important role in many photonics-based technologies since decades. Novel high-power ultrashort-pulse laser and parametric sources, operating at infrared wavelengths, have recently enabled new application areas in nonlinear optics [1,2]. For example, extremely efficient terahertz (THz) pulse generation has been investigated by optical rectification of infrared pump pulses in semiconductors [3–9]. THz-pulse-driven high-harmonic generation, recently demonstrated in GaSe semiconductor [10], may enable to explore and exploit electron wavefunctions and the band structure by all-optical methods, and even lead to the construction of intense CEP-stable solid-state attosecond sources. To design and optimize setups and devices utilizing intense optical driving of semiconductors, the knowledge of their nonlinear optical parameters, such as the nonlinear refractive index or multiphoton absorption coefficients, is very important.

Theoretical scaling laws for multiphoton absorption coefficients have been given for direct-bandgap semiconductors based on a two-band model [11]. An early summary on theoretical models and experimental values of two- (2PA) and three-photon absorption (3PA) coefficients for a few selected materials can be found in [12], Nathan et al. 2PA and 3PA of semiconductors have been extensively studied experimentally in the past. The anisotropy of 2PA in GaAs [13,14] and CdTe [13] has been studied with nanosecond and 30-ps pulses and found to reflect the anisotropy of the band structure because of large 2PA-generated free carrier absorption. The most commonly used method to measure 2PA and 3PA coefficients is the z-scan technique [15]. This has been applied to measure the tensor properties (anisotropy) [16], by using the three nonlinear eigenpolarizations [17], and the dispersion of third-order nonlinearities (2PA) [16,18] in various semiconductors. The dispersion and the anisotropy of 2PA and 3PA in GaAs has been measured

in the 1.3–2.5 μm wavelength range by 100-fs pulses [19]. 3PA spectra have been calculated using a four-band model and compared to measurements in direct-band-gap semiconductors [20,21]. A maximum in the 3PA coefficient has been found both in theory and experiment near the 3PA cut-off wavelength.

In contrast, little is known about the four-photon absorption (4PA) and nonlinearities of even higher order in semiconductors and other important optical materials. Recently, multi-photon absorption in GeSbS chalcogenide glass up to the 11th order has been reported for wavelengths between 1.1 μm and 5.5 μm [22], and values on the order of $10^{-4} \text{ cm}^5\text{GW}^{-3}$ have been found for the 4PA coefficient. The knowledge of 4PA and higher-order nonlinearities can be crucial for applications driven by infrared pulses. For example, in the newly developed very promising semiconductor THz generators, 4PA can be a major design issue [9,23]. The efficiency of THz generation in ZnTe could be increased by two orders of magnitude, from 3.1×10^{-5} [24] to as high as 0.7% [7,8]. The reason for this enormous increase was the elimination of both 2PA and 3PA by a sufficiently long pump wavelength [3,4,6–8,25,26], thereby eliminating the associated free-carrier absorption in the THz range. However, 4PA can still be a limiting factor for THz generation in this case. A first attempt to estimate the 4PA coefficient in ZnTe has been made based on THz generation results [9], but this approach is very indirect and therefore subject to large uncertainties. GaP is another semiconductor nonlinear material of high interest for efficient THz generation [9,23], but no experimental data on its 4PA coefficient are available. Thus, there is a clearly perceived lack of knowledge on important material data.

In this paper, we report on the measurement of the intensity-dependent 4PA coefficient in ZnTe and GaP semiconductors. The anisotropy of the 4PA coefficient is also investigated. For many potential applications of optically driven semiconductors and practical device design, the knowledge of intensity-dependent 4PA coefficients can be indispensable.

2. Experimental setup

Nonlinear transmission measurements with fs pulses have been carried out by using the z-scan technique, which is a widely used method for measuring nonlinear absorption coefficients. The experimental setup is shown in Fig. 1. Pump pulses of $\lambda_0 = 1.75 \mu\text{m}$ central wavelength were delivered at 1 kHz repetition rate by a tuneable optical parametric amplifier (OPA) (Light Conversion, HE TOPAS), driven by a Ti:sapphire laser system (Coherent, Legend Duo). The full width at half maximum of the nearly Gaussian spectral intensity distribution of the pump pulses was about 51 nm. A set of dichroic long-pass filters have been used to suppress possible parasitic spectral components below about 1.65 μm . A pulse duration of 135 fs was measured by autocorrelation.

A spatial filter was used to improve the pump beam quality to nearly Gaussian intensity profile and cylindrical symmetry. The spatial filter consisted of a pair of 400-mm focal-length lenses in a confocal arrangement, and a circular pinhole of 100 μm diameter, placed inside a vacuum chamber with two uncoated windows. A lens with 500 mm focal length was used to focus the beam for the z-scan measurement. The horizontal and vertical beam profiles have been carefully measured by the knife-edge technique at several positions along the propagation direction of the focused beam. The absence of astigmatism has been verified in test z-scan measurements as well. The waist radius of the focused pump beam was $w_0 = 39 \mu\text{m}$ (at $1/e^2$ of the peak intensity). The Rayleigh range was $2z_R = 5.5 \text{ mm}$, significantly larger than the crystal length L . The sample crystal was mounted on a motorized linear stage to move it along the beam propagation direction (z -axis) around the focus. A large-area Ge photodiode of 19.6 mm^2 sensitive area (Thorlabs DET50B/M) was used to measure the power transmitted through the sample. A lens with 100 mm focal length and 25 mm diameter, placed between the sample and the photodiode, was used to avoid closed-aperture effects in the z-scan measurements.

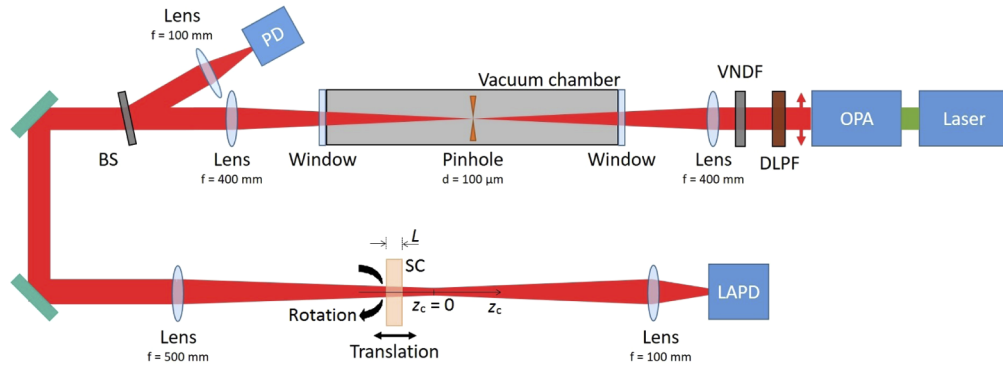


Fig. 1. Experimental setup. OPA: optical parametric amplifier, DLPF: dichroic long-pass filters, VANDF: variable neutral density filter, BS: beam splitter, PD: reference photodiode, SC: semiconductor crystal, LAPD: large-area photodiode.

The laser power transmitted through the sample crystal has been measured as function of the crystal's z-position. Z-scan measurements with GaP and ZnTe crystals have been carried out at various pump energy levels. A step-variable neutral density filter (Thorlabs NDC-100S-4M) was used to attenuate the beam and regulate the pump intensity. In a second measurement series, in order to explore anisotropy effects, the electric-field polarization direction of the linearly polarized pump pulses has been rotated in the plane of the GaP crystal, by rotating the crystal about the beam axis.

The [110]-oriented GaP and ZnTe crystals of 10 mm × 10 mm size and $L = 1$ mm thickness have been measured at room temperature. The GaP crystals were purchased from two different manufacturers (Pi-Kem and Moltech); the ZnTe was from Moltech. Both GaP and ZnTe crystallize in the zincblende structure, $\bar{4}3m$. The (direct) bandgap energies (E_g) of GaP and ZnTe are 2.79 eV and 2.26 eV [27,28], respectively. In GaP, the smaller indirect bandgap of 2.27 eV has been found to play a less important role in multiphoton absorption induced by fs pump pulses [12,28,29], due to the smaller probability of the indirect transition than that of the direct one. The cut-off wavelength for 3PA, $3hc/E_g$, is 1.33 μm for GaP and 1.65 μm for ZnTe. Here, h is the Planck constant and c is the speed of light in vacuum. At pump wavelengths longer than the cut-off, interband linear absorption, 2PA, and 3PA are not effective in the respective material, but 4PA and higher-order multiphoton absorption can still be present. Our choice of 1.75 μm for the pump central wavelength ensured that the entire spectrum was located above the 3PA cut-off wavelength for both materials (for example, the spectral intensity at the 3PA cut-off in ZnTe was less than 2% of the peak intensity). We note that the 4PA cut-off wavelength, $4hc/E_g$, is 1.78 μm for GaP and 2.19 μm for ZnTe. In case of GaP, the long-wavelength wing of the pump spectrum containing about 10% of the pulse energy was located beyond the 4PA cut-off.

3. Theoretical model

A pulse propagation model in the slowly-varying envelope approximation was used, which included the effects of linear dispersion and 4PA inside the crystal. Diffraction and self-focusing effects have been neglected inside the crystal because relatively thin samples were used in the experiment. In the calculation, we have assumed, both in time and space, a Gaussian-shaped pump pulse, incident onto the crystal. The intensity of the pulse just after entering the crystal was given by

$$I(t, z = 0, \rho; z_c) = I_0 \frac{w_0^2}{w^2(z_c)} e^{-4 \ln(2) \frac{t^2}{\tau^2}} e^{-\frac{2\rho^2}{w^2(z_c)}}. \quad (1)$$

Here, t is the time, z ($0 \leq z \leq L$) is the coordinate along the pulse propagation direction inside the crystal, ρ is the radial coordinate, z_c is the coordinate of the input surface of the crystal in the z -scan measurement with $z_c = 0$ corresponding to the focus. The radius at $1/e^2$ of the maximum intensity of the Gaussian beam is $w(z_c)$, the waist radius is w_0 , and the full-width-at-half-maximum pulse duration is τ . I_0 is the peak intensity (maximum in space and time) inside the crystal, taking into account Fresnel losses. The complex electric field envelope inside the crystal is related to the intensity as

$$A(t, z, \rho; z_c) = \sqrt{\frac{2I(t, z, \rho; z_c)}{\epsilon_0 c n_0}}, \quad (2)$$

where ϵ_0 is the vacuum permittivity and n_0 is the refractive index of the crystal at the central frequency of the pulse.

The variation of the intensity due to 4PA is given by the following equation:

$$\frac{d}{dz} I(t, z, \rho; z_c) = -\beta_4 I^4(t, z, \rho; z_c), \quad (3)$$

where β_4 is the 4PA coefficient. Therefore, the effect of 4PA on the field amplitude is given by

$$\frac{d}{dz} A(t, z, \rho; z_c) = -\frac{1}{16} \beta_4 (\epsilon_0 c n_0)^3 A(t, z, \rho; z_c)^7. \quad (4)$$

By using a split-step Fourier method with Δz step size, linear dispersion was accounted for in the spectral domain in the moving frame of the pulse according to the following equation:

$$A(t, z + \Delta z, \rho; z_c) = \mathcal{F}^{-1} \left[\mathcal{F} [A(t, z, \rho; z_c)] e^{i \frac{[n(\omega) - n_g(\omega_0)] \omega}{c} \Delta z} \right]. \quad (5)$$

Here, \mathcal{F} (\mathcal{F}^{-1}) denotes (inverse) Fourier transform, ω is the angular frequency, and $n_g(\omega_0)$ is the group refractive index of the crystal at the $\omega_0 = 2\pi c / \lambda_0$ central frequency of the pulse.

Equations (4) and (5) were numerically solved for different radial coordinates ρ using a split-step Fourier method, similar to that in [30], Yin et al. The z -scan curve, i.e. the normalized transmission T through the sample crystal, as function of the crystal position z_c can be obtained by

$$T(z_c) = \frac{\int_{-\infty}^{\infty} \int_0^{\infty} |A(t, z = L, \rho; z_c)|^2 \rho d\rho dt}{\int_{-\infty}^{\infty} \int_0^{\infty} |A(t, z = 0, \rho; z_c)|^2 \rho d\rho dt}. \quad (6)$$

4. Results and discussion

The results of open-aperture z -scan measurements in [110]-cut GaP and ZnTe crystals, pumped at 1.75 μm wavelength, are shown in Fig. 2. The normalized transmission values refer to those inside the crystal and have been corrected for the Fresnel loss. Negative (positive) z_c values refer to crystal position before (behind) the focus $z_c = 0$. In these measurements, the polarization of the pump pulse was either along the $[\bar{1}11]$ -direction or along the $[1\bar{1}1]$ -direction of the crystals. These directions correspond to the maxima of the second-order nonlinear polarization and are typically used for example in THz generation by optical rectification [7,8]. The intensity values given in the legends refer to peak intensities I_0 at beam centre inside the sample materials.

In case of GaP, Fig. 2(a), the minimum of the measured relative transmission rapidly decreases with increasing pump intensity. At about 150 GWcm^{-2} , saturation of the nonlinear absorption sets on, indicating, besides 4PA, the contribution of other nonlinear effects at higher intensities. In this regime, one can also observe a forward shift of the transmission minima and a change of the shape of the z -scan curves with increasing pump intensity. At the highest intensities ($\geq 300 \text{ GWcm}^{-2}$), the z -scan curves become asymmetric, which is the signature of closed-aperture effect due to

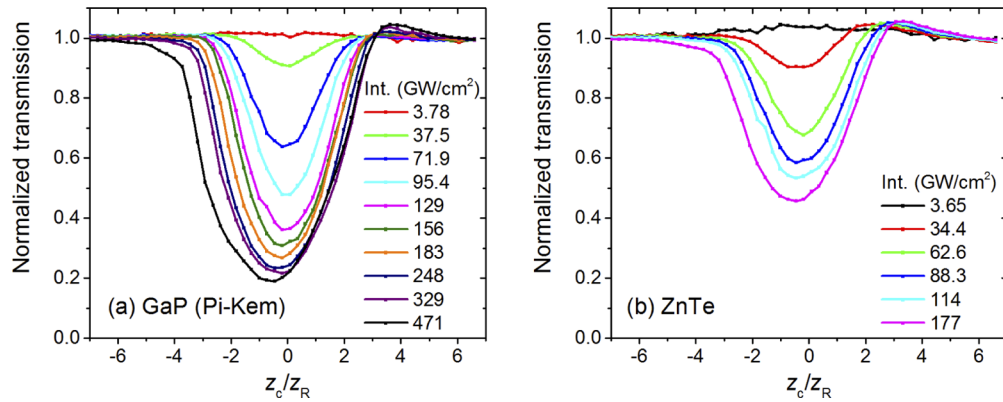


Fig. 2. Measured z-scan curves at various I_0 on-axis peak pump intensity levels for GaP (a) and ZnTe (b).

nonlinear beam reshaping, and can also explain the forward shift of the transmission minima. This was observable despite using an additional positive lens before the detector (see Fig. 1). In case of ZnTe, Fig. 2(b), similar behaviour has been observed, except that the nonlinear change of the transmission is somewhat smaller at comparable intensities and the saturation effect become visible below 100 GWcm^{-2} .

In order to filter out closed-aperture effect at high intensities, the measured z-scan curves have been symmetrized according to $T_s(z_c) = [T(z_c) + T(-z_c)]/2$ [31]. The minima of the measured and symmetrized z-scan curves have been fitted by varying the 4PA coefficient in the nonlinear pulse propagation model described in Section 3. In each case, a few measured data points with the lowest transmission values were considered for fitting the least-square method. The only free parameter in the fitting was the β_4 coefficient. Examples of measured and symmetrized GaP (Pi-Kem) z-scan curves, corresponding to different peak pump intensities, are shown in Fig. 3, together with the calculated curves, using the best-fit 4PA coefficient value. The measured and the calculated z-scan curves are in good agreement in the intensity regime below about 100 GWcm^{-2} , where no saturation of the nonlinear transmission occurs (Fig. 3(a)). No significant closed-aperture effect is observed in this range, as illustrated by the nearly vanishing antisymmetric part of the z-scan curve, $T_a(z_c) = [T(z_c) - T(-z_c)]/2$. The agreement between measured and calculated z-scan data is gradually reduced with the onset of saturation (Figs. 3(b) and 3(c)). In this range, increasing closed-aperture effects are also clearly shown by the increasing amplitudes of the antisymmetric parts. The obtained 4PA coefficients are dependent on the peak pump intensity, which is consistent with the presence of other nonlinear effects besides 4PA. We note that considering the obtained intensity dependence of the 4PA coefficient in calculating the individual z-scan curves could possibly improve the agreement between experimental and calculated z-scan curves. However, this would add significant numerical complexity to the model but would not change the 4PA values because they are obtained from the measured transmission minima. For this reason, such a correction has not been carried out here.

The intensity-dependent 4PA coefficients, obtained from fitting the measured-symmetrized z-scan curves, are shown in Fig. 4 as function of the on-axis peak pump intensity. The numerical values are also shown in the inset table in Fig. 4. In case of GaP, the 4PA coefficient increases monotonically from $2.6 \times 10^{-4} \text{ cm}^5 \text{GW}^{-3}$ at 37.5 GWcm^{-2} pump intensity to its maximum of $56.5 \times 10^{-4} \text{ cm}^5 \text{GW}^{-3}$ at 183 GWcm^{-2} intensity. The maximum is $64.9 \times 10^{-4} \text{ cm}^5 \text{GW}^{-3}$ in case of the Moltech GaP crystal. The maximum is followed by a monotonic decrease at still higher intensities. There was no significant difference between the two GaP crystals. Similar behaviour was found for ZnTe, but the maximum value of the 4PA coefficient was about 6

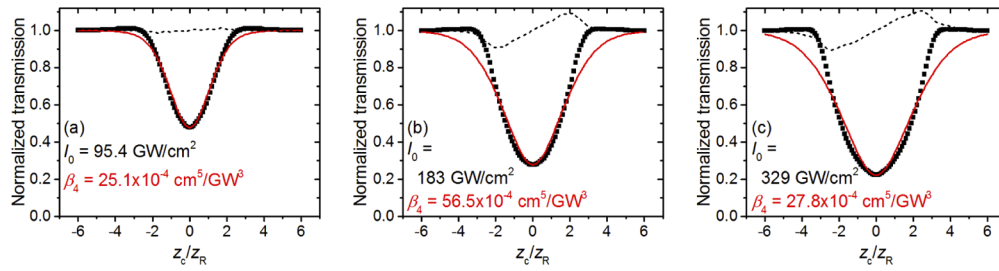


Fig. 3. Examples of symmetrized z-scan curves, measured at different I_0 on-axis peak pump intensities (symbols), and the best-fit calculated curves (solid line) in case of GaP. The dashed lines show the antisymmetric parts of the z-scan curves, shifted by 1 for better visibility.

times smaller, measured at about 3 times lower intensity. The 4PA coefficient increases from $3.5 \times 10^{-4} \text{ cm}^5\text{GW}^{-3}$ at 34.4 GWcm^{-2} intensity to $9.1 \times 10^{-4} \text{ cm}^5\text{GW}^{-3}$ at 63 GWcm^{-2} . At higher intensities, the 4PA coefficient decreases. The knowledge of the intensity-dependent (effective) 4PA coefficients can be useful in designing practical devices and constitute the central result of this work.

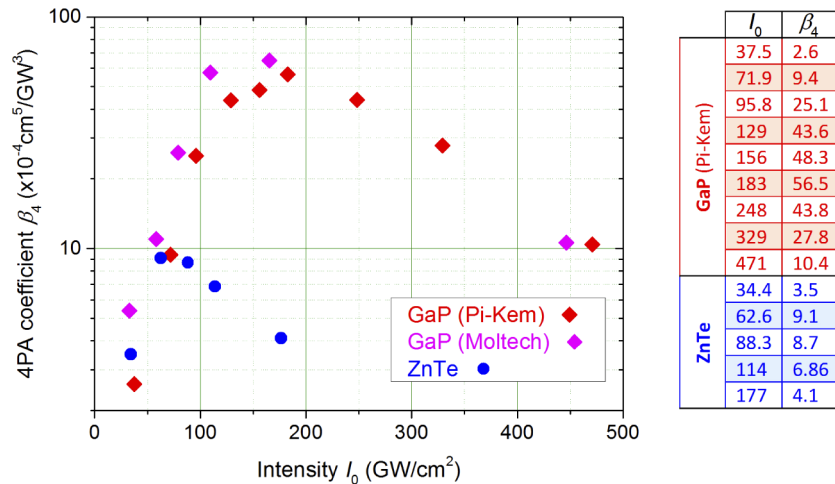


Fig. 4. Intensity-dependent 4PA coefficients as function of the on-axis peak pump intensity. The numerical values in the inset table are given in the same units as in the graph.

The intensity dependence of the determined 4PA coefficients and the occurrence of closed-aperture effect at higher intensities, hinting to strong beam reshaping by nonlinear phase shift, are signatures of additional nonlinear effects not considered in our model. These effects may contribute both to nonlinear absorption as well as the nonlinear refractive index. Nonlinear absorption can be caused by a number of effects, such as five-photon and higher-order multiphoton absorption, the absorption of free carriers generated by multiphoton absorption and tunnel ionization from the valence to the conduction band [10,32], or non-phase-matched second-harmonic generation and eventually subsequent 2PA. Contribution to the nonlinear phase can arise from the nonlinear refractive index n_2 and from free carriers generated by the effects mentioned above [33]. The nonlinear phase can also change the beam size, besides changing the temporal shape, which can lead to the change of the free-space propagation of the beam, but also to the change of the intensity and the nonlinear absorption within the sample.

At higher intensities, free-carrier generation by 4PA can contribute to the nonlinear absorption. Figure 5 shows the estimation of the free-carrier absorption (FCA) coefficient $\alpha_{fc}(\lambda) = 4\pi \cdot \text{Im}[\sqrt{\epsilon_{fc}(\lambda)}]/\lambda$ as function of the intensity. Here, λ is the wavelength and $\epsilon_{fc}(\lambda)$ is the free-carrier contribution to the complex dielectric function [23]. The calculation, which may overestimate FCA, is based on the 4PA coefficients in Fig. 4. According to Fig. 5, $\alpha_{fc} \cdot L > 1$ holds for $L = 1$ mm above about 120 GWcm^{-2} intensity in GaP. This suggests that FCA can contribute to the increase of the 4PA coefficient of GaP at intermediate intensities between about 120 GWcm^{-2} and 200 GWcm^{-2} . Possible saturation of FCA due to the scattering of the free carriers into valleys with low mobility and/or anharmonicity of the valleys causing low mobility of highly excited electrons [34] can contribute to the decrease of the 4PA coefficient observed at still higher intensities. In ZnTe $\alpha_{fc} \cdot L > 1$ holds for $L = 1$ mm above about 170 GWcm^{-2} intensity, and the contribution of FCA and its saturation to the increase and subsequent decrease (above about 70 GWcm^{-2}) of the 4PA coefficient may be less significant. We note that the saturation of FCA in a ZnTe THz source has been reported in [35], Ku et al.

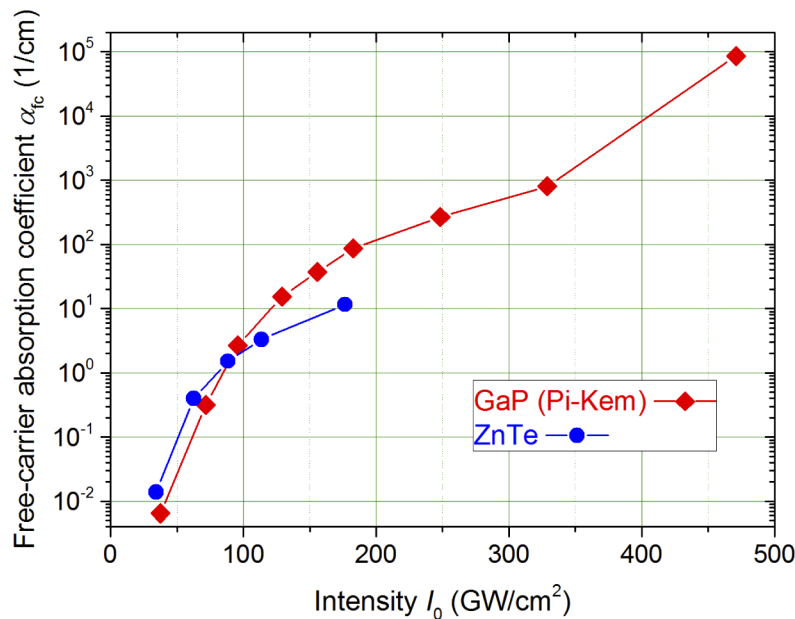


Fig. 5. Estimated free-carrier absorption coefficient as function of the on-axis peak pump intensity.

Non-phase-matched second-harmonic generation, followed by 2PA is estimated to be less likely to contribute. The highest intensity used in case of GaP was 471 GWcm^{-2} , which gives a Keldysh parameter of about 3.2, indicating the absence of strong tunnelling effects. Furthermore, a significant redistribution of the electron population due to the intense excitation can even lead to additional changes of the linear and nonlinear optical parameters, and other material parameters, such as the bandgap. Further experimental and theoretical investigations are needed to clarify possible contributions of the mentioned effects. Such studies, which are beyond the scope of the present work, may include the development of more sophisticated theoretical models and optical pump—THz probe measurements of transient carrier dynamics.

4PA can be a major efficiency-limiting effect in semiconductor THz sources pumped at wavelengths longer than the cut-off for 3PA. In our previous work, we gave the estimation of $(3 \pm 1) \times 10^{-5} \text{ cm}^5 \text{ GW}^{-3}$ for the 4PA coefficient in ZnTe by fitting simulation results to experimental data on THz generation efficiency [9]. The prediction of simulations using this

value of the 4PA coefficient agreed well with the observed saturation of the THz generation efficiency and the maximum efficiency found at 14 GWcm^{-2} pump intensity. However, it is about one order of magnitude smaller than the smallest 4PA coefficient measured here by z-scan at about two times higher intensity (Fig. 4).

In a further z-scan measurement series, the polarization direction of the linearly polarized pump pulses has been varied with respect to the dielectric Z[001]-axis of the [110]-oriented GaP crystal. The pump intensity was 65 GWcm^{-2} . The results, shown in Fig. 6, clearly reveal the anisotropy of the 4PA coefficient, which varies between $3.4 \times 10^{-4} \text{ cm}^5\text{GW}^{-3}$ and $14.5 \times 10^{-4} \text{ cm}^5\text{GW}^{-3}$. The error bar in determining the 4PA coefficient value can be estimated to about 6.5% due to laser intensity fluctuation. The two largest 4PA coefficient values can be seen, at 55° and 135° polarization angles, measured from the Z-axis. The extraordinarily large value at 55° is most probably due to the effect of crystal surface errors or dust. No polarization-dependent z-scan measurements have been carried out with ZnTe here, but a similar behaviour can be expected due to symmetry reasons. We note that the second-order nonlinear susceptibility, responsible for second-harmonic generation (SHG) or optical rectification, also exhibits a qualitatively similar anisotropy (see the red empty symbol and the red dashed curve in Fig. 6 for SHG in GaP, and the Supplementary Material in [8], Fülöp et al. for ZnTe). Its maxima are at 54.7° and 125° (vertical dashed lines in Fig. 6), which are close to the 55° and 135° angles where 4PA maxima were found.

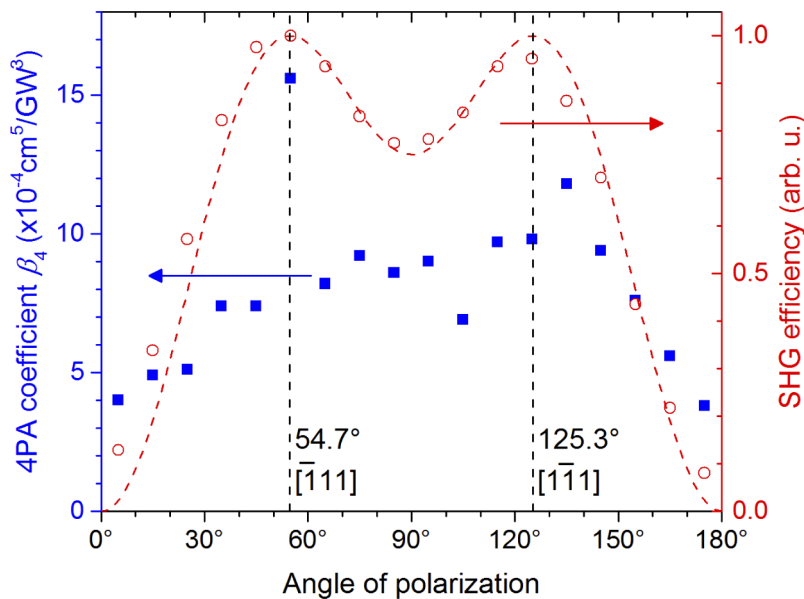


Fig. 6. Measured anisotropy of the 4PA coefficient in GaP (full symbols, left vertical axis) as function of the pump polarization angle. For comparison, the measured (red empty symbols) and calculated (dashed red line) SHG efficiency (right vertical axis) is also shown. The vertical dashed lines indicate the given crystallographic directions.

We note that qualitatively similar anisotropy has been reported for 2PA [14] and 3PA [19] in [110]-oriented GaAs, which has the same symmetry group as GaP and ZnTe. Good agreement was found between 2PA anisotropy measurements of GaAs with ps [14] and ns [13] pulses. In the latter case, 2PA-induced free-carrier absorption was large, and the 2PA anisotropy was found to reflect the anisotropy of the band structure. An expression for the pump polarization dependence of the effective third-order nonlinear susceptibility, relevant for 2PA, can be easily derived from the tensor symmetry properties [14,36]. The description of 3PA anisotropy requires

the knowledge of the symmetry properties of the fifth-order nonlinear susceptibility tensor, which is already sparse in the literature [37,38]. 4PA anisotropy requires to deal with the seventh-order nonlinear susceptibility tensor (of rank 8), which we have not found in the literature. Due to the uncertainties in the exact physical origin and the mathematical complexity, a theoretical discussion of 4PA anisotropy is beyond the scope of this work.

For comparison, we note that an estimation of $10^{-7} \text{ cm}^5 \text{ GW}^{-3}$ has been given for the 4PA coefficient of LiNbO_3 based on THz generation results with $1.03 \mu\text{m}$ pump wavelength [3]. This value is less reliable, as it is dependent on another fitting parameter [3]. The values obtained in the present work for GaP and ZnTe are three to four orders of magnitude larger. 4PA values on the order of $10^{-4} \text{ cm}^5 \text{ GW}^{-3}$ have been reported for GeSbS chalcogenide glass [22], which are of similar order of magnitude than our values for ZnTe. Our values for GaP are of similar order or one order of magnitude larger, depending on intensity. The relatively large values of 4PA coefficients in the investigated semiconductors underlines the importance of their knowledge, because 4PA can be significant even at moderate optical intensities.

It is also noted that we have carried out closed-aperture z-scan measurements at a pump intensity of 57.2 GWcm^{-2} to estimate the nonlinear refractive index at the $1.75 \mu\text{m}$ pump wavelength. A value of $n_2 = 1.9 \times 10^{-18} \text{ m}^2 \text{ W}^{-1}$ was found for GaP and $n_2 = 1.6 \times 10^{-18} \text{ m}^2 \text{ W}^{-1}$ for ZnTe. Values at some other wavelengths can be found in [28], Liu et al. and [39], He et al.

5. Conclusion

Intensity-dependent four-photon absorption (4PA) coefficients in GaP and ZnTe semiconductors have been measured by the z-scan method using pump pulses of $1.75 \mu\text{m}$ wavelength and 135 fs duration. The choice of the pump wavelength longer than the cut-off for 4PA ensured that no interband linear, as well as two- and three-photon absorptions had to be taken into account. The intensity-dependent 4PA coefficients, obtained in a very broad range of pump intensities from about 30 GWcm^{-2} up to about 500 GWcm^{-2} , vary from 2.6×10^{-4} to $65 \times 10^{-4} \text{ cm}^5 \text{ GW}^{-3}$ in GaP, and from 3.5×10^{-4} to $9.1 \times 10^{-4} \text{ cm}^5 \text{ GW}^{-3}$ in ZnTe. The anisotropy of 4PA has been shown in GaP.

The knowledge of 4PA coefficients is important for the design of semiconductor nonlinear optical devices. Prominent examples are extremely efficient monolithic semiconductor THz sources [7–9,23], demonstrated recently, which are potential next-generation drivers for high-field applications such as THz nonlinear spectroscopy and particle acceleration.

Funding

Emberi Erőforrások Minisztériuma (EFOP-3.6.2-16); Eurostars (E 12576 HABRIA); Nemzeti Kutatási Fejlesztési és Innovációs Hivatal (2018-1.2.1-NKP-2018-00009, 2018-2.1.5-NEMZ-2018-00003, NN 125808); Magyar Tudományos Akadémia (János Bolyai Scholarship to Gy. T.); Schweizerischer Nationalfonds zur Förderung der Wissenschaftlichen Forschung (NCCR MUST).

Disclosures

The authors declare no conflicts of interest.

References

1. A. D. Koulouklidis, C. Gollner, V. Shumakova, V. Y. Fedorov, A. Pugžlys, A. Baltuška, and S. Tzortzakis, "Observation of extremely efficient terahertz generation from mid-infrared two-color laser filaments," *Nat. Comm.* **11**, 292 (2020).
2. D. Jain and O. Bang, "High power mid-infrared fiber based supercontinuum sources: Current status and future perspectives," in *2018 Conference on Lasers and Electro-Optics Pacific Rim (CLEO-PR)*, (2018), pp. 1–2.
3. M. C. Hoffmann, K.-L. Yeh, J. Hebling, and K. A. Nelson, "Efficient terahertz generation by optical rectification at 1035 nm," *Opt. Express* **15**(18), 11706–11713 (2007).

4. J. A. Fülöp, L. Pálfalvi, G. Almási, and J. Hebling, "Design of high-energy terahertz sources based on optical rectification," *Opt. Express* **18**(12), 12311–12327 (2010).
5. Z. Ollmann, J. A. Fülöp, J. Hebling, and G. Almási, "Design of a high-energy terahertz pulse source based on ZnTe contact grating," *Opt. Commun.* **315**, 159–163 (2014).
6. F. Blanchard, B. E. Schmidt, X. Ropagnol, N. Thire, T. Ozaki, R. Morandotti, D. G. Cooke, and F. Legare, "Terahertz pulse generation from bulk GaAs by a tilted-pulse-front excitation at 1.8 μm ," *Appl. Phys. Lett.* **105**(24), 241106 (2014).
7. G. Polónyi, B. Monoszlai, G. Gaumann, E. J. Rohwer, G. Andriukaitis, T. Balciunas, A. Pugzlys, A. Baltuska, T. Feurer, J. Hebling, and J. A. Fülöp, "High-energy terahertz pulses from semiconductors pumped beyond the three-photon absorption edge," *Opt. Express* **24**(21), 23872–23882 (2016).
8. J. A. Fülöp, G. Polónyi, B. Monoszlai, G. Andriukaitis, T. Balciunas, A. Pugzlys, G. Arthur, A. Baltuska, and J. Hebling, "Highly efficient scalable monolithic semiconductor terahertz pulse source," *Optica* **3**(10), 1075–1078 (2016).
9. G. Polónyi, M. I. Mechler, J. Hebling, and J. A. Fülöp, "Prospects of semiconductor terahertz pulse sources," *IEEE J. Sel. Top. Quantum Electron.* **23**(4), 1–8 (2017).
10. M. Hohenleutner, F. Langer, O. Schubert, M. Knorr, U. Huttner, S. W. Koch, M. Kira, and R. Huber, "Real-time observation of interfering crystal electrons in high-harmonic generation," *Nature* **523**(7562), 572–575 (2015).
11. B. S. Wherrett, "Scaling rules for multiphoton interband absorption in semiconductors," *J. Opt. Soc. Am. B* **1**(1), 67–72 (1984).
12. V. Nathan, A. H. Guenther, and S. S. Mitra, "Review of multiphoton absorption in crystalline solids," *J. Opt. Soc. Am. B* **2**(2), 294–316 (1985).
13. S. J. Bepko, "Anisotropy of two-photon absorption in GaAs and CdTe," *Phys. Rev. B* **12**(2), 669–672 (1975).
14. R. DeSalvo, M. Sheik-Bahae, A. A. Said, D. J. Hagan, and E. W. Van Stryland, "Z-scan measurements of the anisotropy of nonlinear refraction and absorption in crystals," *Opt. Lett.* **18**(3), 194–196 (1993).
15. M. Sheik-Bahae, A. A. Said, T. Wei, D. J. Hagan, and E. W. Van Stryland, "Sensitive measurement of optical nonlinearities using a single beam," *IEEE J. Quantum Electron.* **26**(4), 760–769 (1990).
16. T. D. Krauss, J. K. Ranka, F. W. Wise, and A. L. Gaeta, "Measurements of the tensor properties of third-order nonlinearities in wide-gap semiconductors," *Opt. Lett.* **20**(10), 1110–1112 (1995).
17. J. Yumoto and K. Otsuka, "Frustrated optical instability: Self-induced periodic and chaotic spatial distribution of polarization in nonlinear optical media," *Phys. Rev. Lett.* **54**(16), 1806–1809 (1985).
18. I. B. Zotova and Y. J. Ding, "Spectral measurements of two-photon absorption coefficients for CdSe and GaSe crystals," *Appl. Opt.* **40**(36), 6654–6658 (2001).
19. W. C. Hurlbut, Y.-S. Lee, K. L. Vodopyanov, P. S. Kuo, and M. M. Fejer, "Multiphoton absorption and nonlinear refraction of GaAs in the mid-infrared," *Opt. Lett.* **32**(6), 668–670 (2007).
20. C. M. Cirloganu, P. D. Olszak, L. A. Padilha, S. Webster, D. J. Hagan, and E. W. Van Stryland, "Three-photon absorption spectra of zinc blende semiconductors: theory and experiment," *Opt. Lett.* **33**(22), 2626–2628 (2008).
21. D. Peceli, P. D. Olszak, C. M. Cirloganu, S. Webster, L. A. Padilha, T. Ensley, H. Hu, G. Nootz, D. J. Hagan, and E. W. Van Stryland, "Three-photon absorption of GaAs and other semiconductors," in *Nonlinear Optics* (Optical Society of America, 2013), p. NTu1B.6
22. B.-U. Sohn, M. Kang, J. W. Choi, A. M. Agarwal, K. Richardson, and D. T. H. Tan, "Observation of very high order multi-photon absorption in GeSbS chalcogenide glass," *APL Photonics* **4**(3), 036102 (2019).
23. P. S. Nugraha, G. Krizsán, G. Polónyi, M. I. Mechler, J. Hebling, G. Tóth, and J. A. Fülöp, "Efficient semiconductor multicycle terahertz pulse source," *J. Phys. B: At., Mol. Opt. Phys.* **51**(9), 094007 (2018).
24. F. Blanchard, L. Razzari, H. C. Bandulet, G. Sharma, R. Morandotti, J. C. Kieffer, T. Ozaki, M. Reid, H. F. Tiedje, H. K. Haugen, and F. A. Hegmann, "Generation of 1.5 μJ single-cycle terahertz pulses by optical rectification from a large aperture ZnTe crystal," *Opt. Express* **15**(20), 13212–13220 (2007).
25. K. L. Vodopyanov, "Terahertz-wave generation with periodically inverted gallium arsenide," *Laser Phys.* **19**(2), 305–321 (2009).
26. K. L. Vodopyanov, M. M. Fejer, X. Yu, J. S. Harris, Y. S. Lee, W. C. Hurlbut, V. G. Kozlov, D. Bliss, and C. Lynch, "Terahertz-wave generation in quasi-phase-matched GaAs," *Appl. Phys. Lett.* **89**(14), 141119 (2006).
27. P. Y. Yu and M. Cardona, *Fundamentals of semiconductors: physics and materials properties* (Springer, 2010).
28. F. Liu, Y. F. Li, Q. R. Xing, L. Chai, M. L. Hu, C. L. Wang, Y. Q. Deng, Q. Sun, and C. Y. Wang, "Three-photon absorption and kerr nonlinearity in undoped bulk GaP excited by a femtosecond laser at 1040 nm," *J. Opt.* **12**(9), 095201 (2010).
29. Y. Li, F. Liu, Y. Li, L. Chai, Q. Xing, M. Hu, and C. Wang, "Experimental study on GaP surface damage threshold induced by a high repetition rate femtosecond laser," *Appl. Opt.* **50**(13), 1958–1962 (2011).
30. Y. Yin, J. Li, X. Ren, Y. Wang, A. Chew, and Z. Chang, "High-energy two-cycle pulses at 3.2 μm by a broadband-pumped dual-chirped optical parametric amplification," *Opt. Express* **24**(22), 24989–24998 (2016).
31. M. Yin, H. Li, S. Tang, and W. Ji, "Determination of nonlinear absorption and refraction by single Z-scan method," *Appl. Phys. B* **70**(4), 587–591 (2000).
32. M. Schultze, K. Ramasesha, C. D. Pemmaraju, S. A. Sato, D. Whitmore, A. Gandman, J. S. Prell, L. J. Borja, D. Prendergast, K. Yabana, D. M. Neumark, and S. R. Leone, "Attosecond band-gap dynamics in silicon," *Science* **346**(6215), 1348–1352 (2014).

33. A. A. Said, M. Sheik-Bahae, D. J. Hagan, T. H. Wei, J. Wang, J. Young, and E. W. Van Stryland, "Determination of bound-electronic and free-carrier nonlinearities in ZnSe, GaAs, CdTe, and ZnTe," *J. Opt. Soc. Am. B* **9**(3), 405–414 (1992).
34. J. Hebling, M. C. Hoffmann, H. Y. Hwang, K.-L. Yeh, and K. A. Nelson, "Observation of nonequilibrium carrier distribution in Ge, Si, and GaAs by terahertz pump–terahertz probe measurements," *Phys. Rev. B* **81**(3), 035201 (2010).
35. S. A. Ku, C. M. Tu, W.-C. Chu, C. W. Luo, K. H. Wu, A. Yabushita, C. C. Chi, and T. Kobayashi, "Saturation of the free carrier absorption in ZnTe crystals," *Opt. Express* **21**(12), 13930 (2013).
36. R. L. Sutherland, D. G. McLean, and S. Kirkpatrick, *Handbook of nonlinear optics*, 2nd ed. (Marcel Dekker, 2003).
37. V. I. Zavelishko, V. A. Martynov, S. M. Saltiel, and V. G. Tunkin, "Optical nonlinear fourth- and fifth-order susceptibilities," *Quantum Electron.* **5**(11), 1392–1393 (1975).
38. S. V. Popov, Y. P. Svirko, and N. I. Zheludev, *Susceptibility Tensors for Nonlinear Optics* (IOP Publishing Ltd., 1995).
39. W.-Q. He, C.-M. Gu, and W.-Z. Shen, "Direct evidence of kerr-like nonlinearity by femtosecond z-scan technique," *Opt. Express* **14**(12), 5476 (2006).